JOURNAL OF GEOPHYSICAL RESEARCH, VOL. 108, NO. D22, 4688, doi:10.1029/2003JD003480, 2003

A generalized single-channel method for retrieving land surface temperature from remote sensing data

Juan C. Jiménez-Muñoz and José A. Sobrino

Global Change Unit, Department of Thermodynamics, Faculty of Physics, University of Valencia, Burjassot, Spain

Received 3 February 2003; revised 27 June 2003; accepted 13 August 2003; published 18 November 2003.

[1] Many papers have developed algorithms to retrieve land surface temperature from at-sensor and land surface emissivity data. These algorithms have been specified for different thermal sensors on board satellites, i.e., the algorithm used for one thermal sensor (or a combination of thermal sensors) cannot be used for other thermal sensor. The main goal of this paper is to propose a generalized single-channel algorithm that only uses the total atmospheric water vapour content and the channel effective wavelength (assuming that emissivity is known), and can be applied to thermal sensors characterized with a FWHM (Full-Width Half-Maximum) of around 1 μm actually operative on board satellites. The main advantage of this algorithm compared with the other single-channel methods is that in-situ radiosoundings or effective mean atmospheric temperature values are not needed, whereas the main advantage of this algorithm compared with split-window and dual-angle methods is that it can be applied to different thermal sensors using the same equation and coefficients. The validation for different test sites shows root mean square deviations lower than 2 K for AVHRR channel 4 ($\lambda \approx 10.8$ μm) and ATSR-2 channel 2 ($\lambda \approx 11$ μm), and lower than 1.5 K for Landsat Thematic Mapper (TM) band 6 ($\lambda \approx 11.5$ μm). *INDEX TERMS:* 1640 Global Change: Remote sensing; 3359 Meteorology and Atmospheric Dynamics: Radiative processes; 3360 Meteorology and Atmospheric Dynamics: Remote sensing; *KEYWORDS:* land surface temperature, single-channel, remote sensing

Citation: Jiménez-Muñoz, J. C., and J. A. Sobrino, A generalized single-channel method for retrieving land surface temperature from remote sensing data, *J. Geophys. Res.*, *108*(D22), 4688, doi:10.1029/2003JD003480, 2003.

1. Introduction

[2] The importance of land surface temperature (LST) for environmental studies has been highlighted by several authors: *Barton* [1992], *Lagouarde et al.* [1995], *Qin and Karnieli* [1999], *Dash et al.* [2002], *Schmugge et al.* [2002], etc. Various algorithms have been developed to retrieve LST from at-sensor and auxiliary data: single-channel methods, split-window technique and multi-angle methods. To apply the last two methods at least two thermal channels are required. The estimation of LST with only one thermal channel is the main advantage for single-channel methods. For example, this is the only method that can be applied to the Landsat platform, with one thermal channel (Thematic Mapper, band 6). Traditionally, the main disadvantage of this method is that some atmospheric parameters are needed, usually by mean of a radiosounding. Our main goal in this paper is to propose a generalized single-channel algorithm that can be applied to different sensors onboard a satellite. This algorithm uses the same minimum input data that the dual-channel and dual-angle algorithms and assumes that land surface emissivity is known: the effective wavelength of the sensor, the atmospheric water vapour content and the at-sensor data (brightness temperature or at-sensor radiance).

2. Theory

[3] On the basis of radiative transfer equation, the at-sensor radiance ($L_\lambda^{\text{at-sensor}}$) for a given wavelength (λ) can be written with a good approximation as

$$L_\lambda^{at-sensor} = \left[\varepsilon_\lambda B(\lambda, T_s) + (1-\varepsilon_\lambda) L_\lambda^{atm\downarrow}\right]\tau_\lambda + L_\lambda^{atm\uparrow} \qquad (1)$$

where ε_λ is the surface emissivity, $B(\lambda,T_s)$ is the radiance emitted by a blackbody at temperature T_s (It should be noted that T_s is the LST mentioned in the paper), $L_\lambda^{atm\downarrow}$ is the down-welling radiance, τ_λ is the total transmission of the atmosphere (transmissivity) and $L_\lambda^{atm\uparrow}$ is the up-welling atmospheric radiance. All these magnitudes also depend on the observation angle. The expression for $B(\lambda, T_s)$ is given by the Planck's law:

$$B(\lambda, T_s) = \frac{c_1 \lambda^{-5}}{\exp\left(\frac{c_2}{\lambda T_s}\right) - 1} \qquad (2)$$

with $c_1 = 1.19104 \cdot 10^8$ w μm^4 m^{-2} sr^{-1} and $c_2 = 1.43877 \cdot 10^4$ μm K, $B(\lambda, T_s)$ is given in w m^{-2} sr^{-1} μm^{-1} if λ is given in μm.

Copyright 2003 by the American Geophysical Union.
0148-0227/03/2003JD003480$09.00

[4] It is difficult to obtain from Equations (1) and (2) an operative expression for T_s. However, a linear relationship between radiance and temperature can be found from the Taylor's approximation around a certain temperature value (T_o):

$$B(\lambda, T_s) = B(\lambda, T_o) + \left[\frac{\partial B(\lambda, T_s)}{\partial T_s}\right]_{\lambda, T_s = T_o} (T_s - T_o) \equiv \alpha(\lambda, T_o) + \beta(\lambda, T_o) T_s \quad (3)$$

where

$$\alpha(\lambda, T_o) \equiv B(\lambda, T_o) - \left[\frac{\partial B(\lambda, T_s)}{\partial T_s}\right]_{\lambda, T_s = T_o} T_o$$

$$= B(\lambda, T_o)\left[1 - \frac{c_2}{T_o}\left(\frac{\lambda^4}{c_1} B(\lambda, T_o) + \frac{1}{\lambda}\right)\right] \quad (4a)$$

$$\beta(\lambda, T_o) \equiv \left[\frac{\partial B(\lambda, T_s)}{\partial T_s}\right]_{\lambda, T_s = T_o} = \frac{c_2 B(\lambda, T_o)}{T_o^2}\left[\frac{\lambda^4}{c_1} B(\lambda, T_o) + \frac{1}{\lambda}\right] \quad (4b)$$

From Equations (1) and (3), and taking into account that the atmospheric parameters (τ_λ, $L_\lambda^{atm\downarrow}$ and $L_\lambda^{atm\uparrow}$) depend mainly on the atmospheric water vapour content (w) in the thermal infrared region, it is possible to obtain the following equation:

$$Ts = \gamma(\lambda, T_o)\left\{\varepsilon_\lambda^{-1}\left[\psi_1(\lambda, w) L_\lambda^{at-sensor} + \psi_2(\lambda, w)\right] + \psi_3(\lambda, w)\right\} + \delta(\lambda, T_o) \quad (5)$$

In this equation there is a dependence on two parameters obtained from the linear approximation of the Planck's law, γ and δ, and a dependence on three functions obtained from the atmospheric parameters, ψ_1, ψ_2 and ψ_3 (hereinafter referred to as the atmospheric functions), given by

$$\gamma(\lambda, T_o) \equiv \frac{1}{\beta(\lambda, T_o)}; \delta(\lambda, T_o) \equiv -\frac{\alpha(\lambda, T_o)}{\beta(\lambda, T_o)} \quad (6)$$

$$\psi_1(\lambda, w) \equiv \frac{1}{\tau(\lambda, w)}; \psi_2(\lambda, w) \equiv -L^{atm\downarrow}(\lambda, w) - \frac{L^{atm\uparrow}(\lambda, w)}{\tau(\lambda, w)}; \psi_3(\lambda, w) \equiv L^{atm\downarrow}(\lambda, w) \quad (7)$$

(in all the equations the radiances are given in w m^{-2} sr^{-1} μm^{-1}, the temperatures in K, the wavelength in μm and the water vapour content in g/cm^2).

[5] The dependence on the water vapour content is due to that this atmospheric component is the main absorber in the thermal infrared region. It should be noted that up-welling and down-welling radiances also depends on other parameters as mean atmospheric temperature, surface pressure, etc. However, in order to obtain an expression for the atmospheric functions, a simulation has been carried out, as will be explained in the next section (see section 3). In this simulation standard atmospheres has been considered. These atmospheres have been characterized by their atmospheric water vapour content. So the dependence on the other parameters are implicitly included in the numerical coefficients obtained from the simulation procedure.

[6] To obtain LST from Equation (5), five input data are needed (assuming that the expressions for the atmospheric functions are known):

[7] i) Land Surface Emissivity (ε_λ): can be obtained using different methods as the Becker and Li's day/night method [*Becker and Li*, 1995], the Thermal SWIR Radiance Ratio Model and the Δday method [*Goïta and Royer*, 1997], the NDVI thresholds method [*Sobrino and Raissouni*, 2000], the Temperature and Emissivity Separation method [*Gillespie et al.*, 1998], etc.

[8] ii) At-sensor radiance ($L_\lambda^{at\text{-}sensor}$): this magnitude is known, so is the measurement carried out by the sensor (In fact, the measurement given by the sensor are the Digital Counts, and a calibration is needed in order to obtain the physical magnitude called radiance).

[9] iii) A temperature value near to the LST value (T_o): this value can be chosen as an initial estimation of the surface temperature obtained with some methods (for example split-window or dual-angle algorithms) as is proposed by *Gu and Gillespie* [2000]. Other possibility is to choose T_o as the at-sensor brightness temperature ($B(\lambda, T_o) \equiv L_\lambda^{at\text{-}sensor}$) if the atmospheric effect in not so significant (low atmospheric water vapour content).

[10] iv) Atmospheric water vapour content (w): can be obtained from satellite data using different methods [*Gao and Goetz*, 1990a, 1990b; *Kaufman and Gao*, 1992; *Gao et al.*, 1993; *Sobrino et al.*, 2003, etc.]. The atmospheric water vapour content can be also measured in situ using manual sunphotometers as Microtops II or photometric systems as CIMEL318-2 [P. Utrillas, personal communication, 2003] or Multi-Filter Rotating Shadowband Radiometer-MFRSR [*Prata*, 2000].

[11] v) Wavelength for the channel considered (λ): this value must be calculated as an effective wavelength for the channel having the characteristic response function $f(\lambda)$ with the following equation:

$$\lambda_{eff} = \frac{\int \lambda f(\lambda) d\lambda}{\int f(\lambda) d\lambda} \quad (8)$$

If the filter response, $f(\lambda)$, is not available, the central wavelength can be also used, but worse results will be expected. To sum up, to retrieve LST from Equation (5), land surface emissivity and water vapour content values are only needed.

3. Obtaining the Atmospheric Functions by Means of a Simulation

[12] As has been commented in the previous section, the atmospheric functions (ψ_1, ψ_2 and ψ_3) must be obtained by a simulation procedure. The MODTRAN 3.5 radiative transfer code [*Abreu and Anderson*, 1996] has been used to predict the atmospheric parameters (τ_λ, $L_\lambda^{atm\downarrow}$ and $L_\lambda^{atm\uparrow}$) for different atmospheric profiles. For this purpose,

a set of around 60 radiosoundings have been extracted from the TOVS Initial Guess Retrieval (TIGR) database [*Scott and Chedin*, 1981] and used as input data in the MODTRAN code. These radiosoundings cover the variability of surface temperature (from 250 K to 320 K) and atmospheric water vapour content (from 0.15 g/cm^2 to 6.71 g/cm^2) on a world-wide scale. Two different types of attenuation of the surface radiance have been considered: 1) the attenuation produced by water vapour only with profiles given in TIGR radiosoundings, and 2) that produced by both the water vapour profile data and the uniformly mixed gases (CO_2, N_2O, O_3, CO and CH_4) included in the standard atmospheres of the MODTRAN 3.5 code [*Sobrino et al.*, 1993a]. The MODTRAN 3.5 code has been executed in thermal radiance mode for a view angle of nadir and for clear-sky conditions (no aerosols effect).

[13] The results obtained with MODTRAN 3.5 are spectral values, while the sensor on board a satellite measures with finite banded radiometers having the characteristic response function f(λ), so the measurement carried out by the sensor is a weighted average value $\langle x_\lambda \rangle$ given by

$$\langle x_\lambda \rangle = \frac{\int x(\lambda) f(\lambda) d\lambda}{\int f(\lambda) d\lambda} \tag{9}$$

where x is any spectral parameter considered as radiance and transmissivity. The main goal of the single-channel algorithm proposed in this paper is the general use for any sensor on board a satellite, so we propose a general response function (called Gaussian-Triangular filter and abbreviated as GT filter) with a full-width half-maximum (FWHM) value of 1 μm (see Table 1). The expression for the response function has been obtained taking into account a mixed function composed by a gaussian and a triangle function to avoid the infinite contribution of the guassian tails (see Figure 1):

$$f^{GT}(\lambda) = \begin{cases} (\lambda - \lambda_o) + 1 \Rightarrow \lambda_o - 1 < \lambda < \lambda_o - 0.5 \\ \exp\left[\dfrac{-(\lambda - \lambda_o)^2}{0.3607}\right] \Rightarrow \lambda_o - 0.5 < \lambda < \lambda_o + 0.5 \\ (\lambda_o - \lambda) + 1 \Rightarrow \lambda_o + 0.5 < \lambda < \lambda_o + 1 \end{cases} \tag{10}$$

where λ_o is the central wavelength (in μm).

Table 1. Effective Wavelength and Full-width-Half-maximum (FWHM) Values for Some Typical Thermal Sensors Used in Remote Sensing

Platform	Sensor	FWHM, μm	$\lambda_{effective}$, μm
LANDSAT 5	TM-6	2.1	11.457
NOAA-14	AVHRR-4	1.0	10.789
NOAA-14	AVHRR-5	1.0	12.004
ERS 2	ATSR2-11	1.0	10.944
ERS 2	ATSR2-12	1.0	12.065
ENVISAT	AATSR-11	0.9	10.857
ENVISAT	AATSR-12	1.0	12.051
TERRA	ASTER-13	0.7	10.659
TERRA	ASTER-14	0.7	11.289
TERRA	MODIS-31	0.5	11.015
TERRA	MODIS-32	0.5	12.041
MOS	VTIR	1.0	11.000[a]
MOS	VTIR	2.0	11.500[a]
Nimbus 7	CZCS-6	2.0	11.500[a]

[a]Central wavelength.

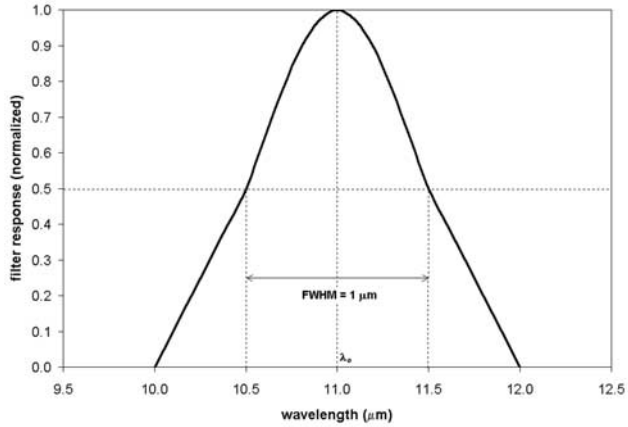

Figure 1. Gaussian-Triangular (GT) filter centered at 11 μm with a full-width-half-maximum (FWHM) value of 1 μm.

[14] Once the simulated filter response has been obtained, a convolution has been applied to all the predicted atmospheric parameters (τ_λ, $L_\lambda^{atm\downarrow}$ and $L_\lambda^{atm\uparrow}$) according to the following equation:

$$\langle \tau_\lambda \rangle = \int f(\lambda - \lambda')\tau(\lambda') d\lambda' \tag{11}$$

(the same expression can be applied to $L_\lambda^{atm\downarrow}$ and $L_\lambda^{atm\uparrow}$). Figure 2 illustrates the spectral transmissivity values (in the 8–13 μm region) simulated with MODTRAN 3.5 and the convolved ones using the Equation (11), in which a smoothed curve is observed.

[15] From convolved values of the atmospheric parameters and Equation (7), it is easy to obtain the atmospheric functions for every wavelength and for every atmospheric water vapour content. Once the atmospheric functions values have been obtained, the objective is to find the explicit dependence for these functions with the atmospheric water vapour content and the wavelength from the

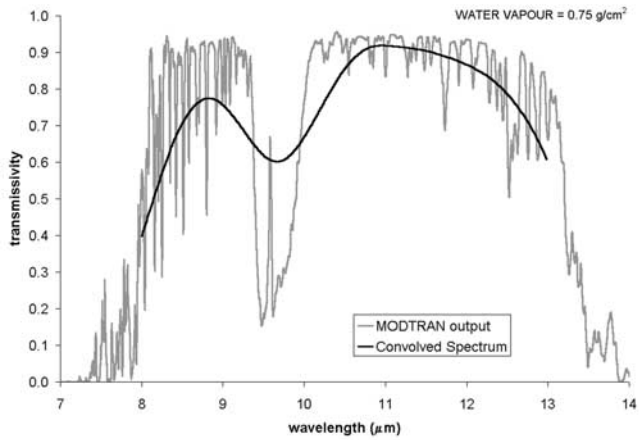

Figure 2. Transmissivity spectrum obtained with MODTRAN 3.5 and convolved transmissivity using the GT filter for an atmosphere with a water vapour content of 0.75 g/cm^2.

Table 2. Numerical Expression for the Atmospheric Functions According to Equation (12) and Equation (13a) From Equation (13d)[a]

AF	Spectral Functions	R
ψ_1	$\eta_{1\lambda} = 0.00090\,\lambda^3 - 0.01638\,\lambda^2 + 0.04745\,\lambda + 0.27436$	0.992
	$\xi_{1\lambda} = 0.00032\,\lambda^3 - 0.06148\,\lambda^2 + 1.2021\,\lambda - 6.2051$	
	$\chi_{1\lambda} = 0.00986\,\lambda^3 - 0.23672\,\lambda^2 + 1.7133\,\lambda - 3.2199$	
	$\varphi_{1\lambda} = -0.15431\,\lambda^3 + 5.2757\,\lambda^2 - 60.1170\,\lambda + 229.3139$	
ψ_2	$\eta_{2\lambda} = -0.02883\,\lambda^3 + 0.87181\,\lambda^2 - 8.82712\,\lambda + 29.9092$	0.993
	$\xi_{2\lambda} = 0.13515\,\lambda^3 - 4.1171\,\lambda^2 + 41.8295\,\lambda - 142.2782$	
	$\chi_{2\lambda} = -0.22765\,\lambda^3 + 6.8606\,\lambda^2 - 69.2577\,\lambda - 233.0722$	
	$\varphi_{2\lambda} = 0.41868\,\lambda^3 - 14.3299\,\lambda^2 + 163.6681\,\lambda - 623.5300$	
ψ_3	$\eta_{3\lambda} = 0.00182\,\lambda^3 - 0.04519\,\lambda^2 + 0.32652\,\lambda - 0.60030$	0.996
	$\xi_{3\lambda} = -0.00744\,\lambda^3 + 0.11431\,\lambda^2 + 0.17560\,\lambda - 5.4588$	
	$\chi_{3\lambda} = -0.00269\,\lambda^3 + 0.31395\,\lambda^2 - 5.5916\,\lambda + 27.9913$	
	$\varphi_{3\lambda} = -0.07972\,\lambda^3 + 2.8396\,\lambda^2 - 33.6843\,\lambda + 132.9798$	

[a]AF, Atmospheric funcion; R, correlation.

simulated database. For this purpose, three-degree expressions are proposed in the following way:

$$\psi_k = \eta_{k\lambda} w^3 + \xi_{k\lambda} w^2 + \chi_{k\lambda} w + \varphi_{k\lambda} (k = 1, 2, 3) \quad (12)$$

where $\eta_{k\lambda}$, $\xi_{k\lambda}$, $\chi_{k\lambda}$ and $\varphi_{k\lambda}$ are spectral functions with three-degree dependence on the wavelength:

$$\eta_{k\lambda} = a_3^{(k)}\lambda^3 + a_2^{(k)}\lambda^2 + a_1^{(k)}\lambda + a_0^{(k)} \quad (13a)$$

$$\xi_{k\lambda} = b_3^{(k)}\lambda^3 + b_2^{(k)}\lambda^2 + b_1^{(k)}\lambda + b_0^{(k)} \quad (13b)$$

$$\chi_{k\lambda} = c_3^{(k)}\lambda^3 + c_2^{(k)}\lambda^2 + c_1^{(k)}\lambda + c_0^{(k)} \quad (13c)$$

$$\varphi_{k\lambda} = d_3^{(k)}\lambda^3 + d_2^{(k)}\lambda^2 + d_1^{(k)}\lambda + d_0^{(k)} \quad (13d)$$

The statistical fits for the whole thermal infrared region [8–14 μm] provide results not accurate enough, so two subregions have been considered: [8–10 μm] and [10–12 μm]. The numerical coefficients ($a_j^{(k)}$, $b_j^{(k)}$, $c_j^{(k)}$, $d_j^{(k)}$; j = 0, 3 and k = 1, 3) obtained with statistical fits in the region [10–12 μm] are showed in Table 2. The numerical coefficients obtained for the region [8–10 μm] are not presented, so all the thermal sensors used in the validation do not work in this region (see section 5). From Equation (12), Equations (13a) to (13d) and the data showed in Table 2 it is possible to calculate the atmospheric functions using effective wavelength and atmospheric water vapour content as input data, and then retrieve the LST from Equation (5).

4. Sensitivity Analysis

[16] In order to apply the single-channel method proposed in the paper, land surface emissivity, atmospheric water vapour, effective wavelength and at-sensor brightness temperatures (or at-sensor radiances) are needed. Errors on these parameters will lead to errors on the LST. To analyze the impact of these errors on the LST retrieved with generalized the single-channel method, the following equation is used:

$$\delta T_s = |T_s(x + \delta x) - T_s(x)| \quad (14)$$

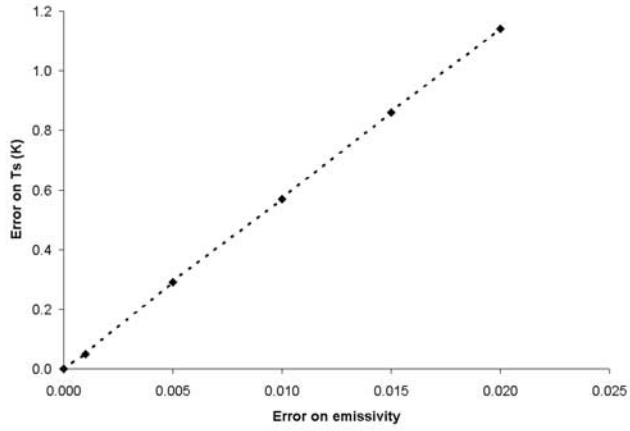

Figure 3. Errors on land surface temperature (T_s) due to the errors on the land surface emissivity.

where δT_s is the error on the LST, x is the parameter for which the sensitivity analysis is performed and δx is the error on this parameter. $T_s(x + \delta x)$ and $T_s(x)$ indicates the LST obtained with the single-channel algorithm when a value of $x + \delta x$ and x is considered, respectively. In order to carry out the sensitivity analysis, an standard atmosphere extracted from the TIGR database with the following conditions has been considered: at-sensor brightness temperature, 297.96 K, land surface temperature, 302.55 K, atmospheric water vapour content, 1.6 g/cm^2, land surface emissivity, 0.969 and effective wavelength, 11 μm. In Figure 3 it is shown the error on the LST due to the emissivity error. As an example, an error on emissivity of 0.01 leads to an error on the LST of around 0.6 K. Figure 4 shows the error on the LST due to the errors on the effective wavelength, the atmospheric water vapour content and the at-sensor brightness temperature (also called noise error). As it is shown in this figure, a wavelength error of 0.3 μm leads to an error on the LST of 0.5 K, while an error of 0.5 g/cm^2 on the atmospheric water vapour leads to an error on the LST of around 0.3 K. Most sensors have a noise error between 0.1 K (AVHRR) and 0.3 K (ASTER), which leads

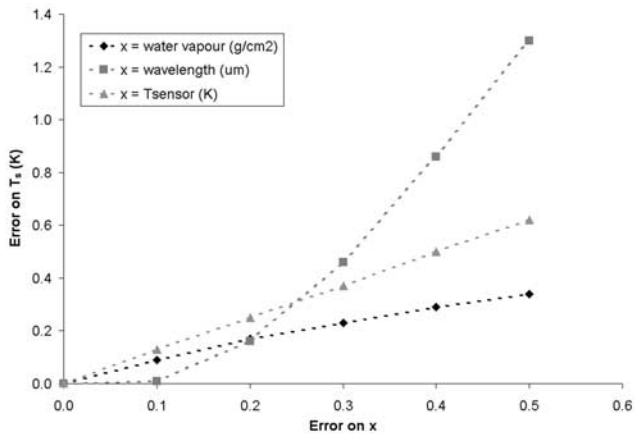

Figure 4. Errors on land surface temperature (T_s) due to the errors on the atmospheric water vapour content, the effective wavelength and the at-sensor brightness temperature.

Table 3. Validation of the Generalized Single-Channel Equation[a]

Sensor	Test Site	Number Data	W, g/cm^2	Bias, K	σ, K	rmsd, K
AVHRR-4	Hay, Walpeup (Australia)	309	0.8–1.2	0.19	1.57	1.58
AVHRR-5	Hay, Walpeup (Australia)	309	0.8–1.2	1.36	1.92	2.35
ATSR2-11	Uardry (Australia)	36	0.6–2.1	0.66	1.87	1.98
ATSR2-12	Uardry (Australia)	36	0.6–2.1	1.88	2.02	2.76

[a]σ, standard deviation; rmsd, root mean square deviation.

to an error on the LST between 0.1 K and 0.4 K. The ATSR sensor has a noise error less than 0.1 K, which leads to a negligible error on the LST.

5. Validation

[17] In order to validate the methodology proposed in this paper, the following thermal sensors and test sites with in-situ LST data set have been chosen:

[18] a) SENSORS: AVHRR channels 4 and 5 onboard NOAA-11 and NOAA-12 (called as AVHRR-4 and AVHRR-5), ATSR2 channels 1 and 2 onboard ERS-2 (called as ATSR2-12 and ATSR2-11), and Landsat Thematic Mapper band 6 onboard LANDSAT (called as TM-6).

[19] b) SITES: Hay, Walpeup and Uardry in Australia [*Prata*, 1994], Requena-Utiel in Spain [*Sobrino et al.*, 1997b; *Boluda et al.*, 1998] and central Canada [*Sellers et al.*, 1995].The results obtained for the Australian database are shown in Table 3, with standard deviations of 1.6 K, 1.9 K, 1.9 K and 2 K for AVHRR-4, AVHRR-5, ASTSR2-11 and ASTR2-12, respectively. For AVHRR-5 and ASTR2-12 high bias values have been also obtained: 1.4 K and 1.9 K, respectively. It should be noted that the in situ LST values have been obtained from vegetation and soil temperatures measured in situ according to the fraction of bare soil and vegetation inside the field of view of the field radiometer, as is explained in [*Prata*, 1994]. The comparison between the results obtained with the same sensor but different wavelength allow us to extract the following remarks:

[20] 1) AVHRR-4 versus AVHRR-5: the LST retrieved with AVHRR-4 data gives lower bias and standard deviation values compared with AVHRR-5 ones. In terms of root mean square deviation (rmsd), a value of 1.6 K for AVHRR-4 and a value of 2.4 K for AVHRR-5 has been obtained. The results obtained with AVHRR-4 agree with typical split-window algorithms developed for NOAA-AVHRR and applied to the same data set [*Sobrino et al.*, 1998]. For example, the algorithm proposed in this paper improves the results obtained using the split-window algorithms developed by *Prata and Platt* [1991], *Price* [1984], *Ulivieri et al.* [1992], *Sobrino et al.* [1993b] and *May et al.* [1992], with rmsd values of 2.1 K, 2.6 K, 1.9 K, 1.7 K and 2.9 K, respectively. The same rmsd value (1.6 K) is obtained from the Becker and Li's algorithm [*Becker and Li*, 1990]. However, the algorithm developed by *Sobrino and Raissouni* [2000] gives a lower rmsd value, of around 1.3 K.

[21] 2) ATSR2-11 versus ATSR2-12: the LST retrieved with ATSR2-11 data gives a lower rmsd value, of around 2 K, compared with the ATSR2-12 one, of around 2.8 K. This result agrees with the one obtained with split-window algorithms developed for ASTR2 [*Sobrino et al.*, 2003], of around 1.9 K. It is possible to improve the results using dual-angle algorithms, which provides rmsd values of 1.3 K and 1.1 K.

[22] According to the results obtained, sensors with effective wavelengths near to 11 μm are more adequate to retrieve LST with a single-channel method than sensors with effective wavelengths near to 12 μm. Although the LST should be theoretically the same for different wavelengths, the higher absorption at wavelengths near to 12 μm in comparison with wavelengths near to 11 μm introduces higher errors on the LST retrieval. In a similar way, it is expected to obtain higher errors when the atmospheric water vapour content is high, so in this case the atmospheric absorption is greater. This fact is observed in the validation of the BOREAS (BOReal forest Ecosystem Study) data. The BOREAS field measurements were collected during the summer of 1994 and encompassed a one million square kilometer region in central Canada. The measurements were carried out coinciding with the NOAA11-AVHRR overpass. In Table 4 it is shown the results obtained for the validation using the generalized single-channel method proposed in the paper for different atmospheric water vapour contents. As the region is a mixture of lakes, coniferous and deciduous forests, an emissivity equal to 0.99 has been chosen for each wavelength. The atmospheric water vapour content varies from 0.05 g/cm^2 to 5.4 g/cm^2. When all the data are considered, a rmsd value of 5 K for AVHRR-4 is obtained. However, a great improvement is achieved when only data with atmospheric water vapour content from 0.05 g/cm^2 to 3 g/cm^2 is considered. In this case, a rmsd value of 1.8 K is obtained for AVHRR-4. The deviation between LST measured in situ and the one obtained from the split-window algorithms proposed by *Ulivieri et al.* [1994] and *Sobrino et al.* [1997a] was less than 4 K for all the cases. This fact illustrates the influence of the atmospheric water vapour content on the error of the LST retrieved with a single-channel method.

[23] With regard to Landsat TM-6 data, only values of emissivity measured in situ and radiosounding data were available. From at-sensor data extracted from the Landsat image, emissivity values and atmospheric parameters obtained from the radiosounding and the MODTRAN 3.5 code, values of LST has been reproduced using Equation (1).

Table 4. Validation of the Generalized Single-Channel Equation From the BOREAS Experiment and AVHRR Data[a]

	Number	AVHRR-4			AVHRR-5		
w, g/cm^2	Data	Bias, K	σ, K	rmsd, K	Bias, K	σ, K	rmsd, K
0.05–5	110	2.33	4.46	5.03	5.47	7.30	9.12
<4	100	1.41	3.16	3.46	4.10	5.25	6.67
<3	82	0.51	1.72	1.79	2.69	2.50	3.67
<2	57	0.18	1.59	1.60	2.15	2.02	2.95

[a]σ, standard deviation; rmsd, root mean square deviation.

Table 5. Validation of the Generalized Single-Channel Equation and Comparison With the Algorithm Developed by *Qin et al.* [2001] Using Landsat TM-6 Data Acquired Over Requena-Utiel (Spain)[a]

Plot	T_{sensor}, K	$\varepsilon_{in\ situ}$	T_s^{situ}, K	T_s^{situ}-T_s^{Qin}, K	$T_s^{situ}-T_s^{Qin\text{-}rad}$, K	$T_s^{situ}-T_s^{gsch}$, K
Reddish soil	307.81	0.974	313.66	−2.43	0.55	−1.29
Light soil	306.24	0.948	313.48	−2.19	0.67	−1.50
Brown soil	307.72	0.962	314.35	−2.36	0.63	−1.37
Vine	306.98	0.990	311.63	−2.48	0.43	−1.23
Mixed soil	308.53	0.967	314.99	−2.43	0.63	−1.32
Clayish soil	308.24	0.966	314.70	−2.41	0.62	−1.33
Mount site	302.60	0.984	306.74	−2.52	−0.02	−1.09
Bias				−2.40	0.50	−1.30
σ				0.11	0.25	0.13
rmsd				2.41	0.56	1.31

[a]The atmospheric data for the day of the acquisition of the Landsat image are the following: atmospheric transmissivity is 0.818, air temperature is 302.55 K, atmospheric temperature = 287.37 K, atmospheric water vapour content = 1.181 g/cm^2. $\varepsilon_{in\ situ}$, emissivity measured in situ at 11 μm; T_s^{situ}, LST obtained from in situ emissivity and radiosounding data using the radiative transfer equation; T_s^{Qin}, LST obtained from the Qin et al's algorithm; $T_s^{Qin\text{-}rad}$, LST obtained from the Qin et al's algorithm using radiosounding data; T_s^{gsch}, LST obtained from the generalized single-channel method proposed in the paper; σ, standard deviation; rmsd, root mean square deviation.

It should be noted that the LST obtained in this way assumes a well calibration of the sensor, which is not always true. The results obtained for the LANDSAT/TM-6 sensor have been compared with the ones obtained using the mono-window algorithm developed by *Qin et al.* [2001], in which air temperature is needed in order to calculate the mean atmospheric temperature (see Table 5). Qin et al.'s algorithm provides low standard deviation values, of around 0.1 K, but high bias values, of around −2.4 K, which means a rmsd value of 2.4 K. The generalized single-channel equation proposed in the paper provides a similar standard deviation value (0.1 K) but improves the bias (−1.3 K), with a final value for rmsd of 1.3 K. As is expected, Qin et al.'s algorithm provides better results when the mean atmospheric temperature is estimated from the in-situ radiosounding data. In this case, low bias, standard deviation and rmsd values are obtained, 0.5 K, 0.3 K and 0.6 K respectively. However, it is possible to improve lightly these results using the methodology presented in the paper, as will be shown bellow (see section 6.1).

[24] It should be noted that the main error source in the methodology proposed is the assumption of an ideal filter response (with a FWHM of 1 μm) for all the thermal sensors. Despite of the filter response for many typical thermal sensors shows significant differences with the GT filter (see Figure 5), the results obtained in the validation agree with the results obtained with other methods to retrieve LST.

6. Particularized Expressions

[25] Equation (12), (13a) to (13d) and Table 2 can be used to obtain general atmospheric functions, i.e., for any thermal channel working in the 10–12 μm region. However, there are some particular cases in which the expressions proposed in the paper can be simplified and easily applied. These cases are discussed in this section.

6.1. Atmospheric Functions for Landsat TM-6

[26] In Section 3 the numerical coefficients for the atmospheric functions depending on the wavelength and the atmospheric water vapour content have been obtained using an ideal filter response. However, Figure 3c shows significant differences between the TM-6 filter response and the GT filter one. It is possible to obtain the appropriate atmospheric functions for Landsat TM-6 using the TM-6 filter response instead of the GT filter response. It should be noted that the numerical coefficients obtained are only applicable to a particular sensor and the general application of the single-channel equation is losed, but it is expected to obtain more accurate values. The following atmospheric functions have been obtained for Landsat TM-6:

$$\psi_1^{TM6} = 0.14714\ w^2 - 0.15583\ w + 1.1234 \tag{15a}$$

$$\psi_2^{TM6} = -1.1836\ w^2 - 0.37607\ w - 0.52894 \tag{15b}$$

$$\psi_3^{TM6} = -0.04554\ w^2 + 1.8719\ w - 0.39071 \tag{15c}$$

The validation carried out using these atmospheric functions shows a rmsd value of 0.5 K, improving the one obtained with the general atmospheric functions (1.3 K, see Table 5). As has been commented in the validation section (see section 5), the LST in situ used for validating Landsat TM-6 data has been estimated assuming a well calibration of the sensor, so the rmsd value obtained indicates the accuracy of the approximations involved in the development of the generalized single-channel method. This result checks up the validity of the linear approximation of the Planck's law if a good value of T_o (see Equation 3) is chosen.

[27] The methodology presented in this section can be used to obtain specific atmospheric functions for the thermal channels of any sensor. In this way, more accurate values are expected, but generality is losed, so these functions can be only applied to particular sensors.

6.2. Sea Surface Temperature (SST) Retrieval

[28] Assuming an emissivity equal to the unity for water, Equation (5) can be simplified as:

$$Ts \approx \gamma(\lambda, T_o)\left[\psi_1^{SST}(\lambda, w)L_\lambda^{at-sensor} + \psi_2^{SST}(\lambda, w)\right] + \delta(\lambda, T_o) \tag{16}$$

In this case, the atmospheric functions are given by

$$\psi_1^{SST}(\lambda, w) \equiv \frac{1}{\tau(\lambda, w)}; \psi_2^{SST}(\lambda, w) \equiv -\frac{L^{atm\uparrow}(\lambda, w)}{\tau(\lambda, w)} \tag{17}$$

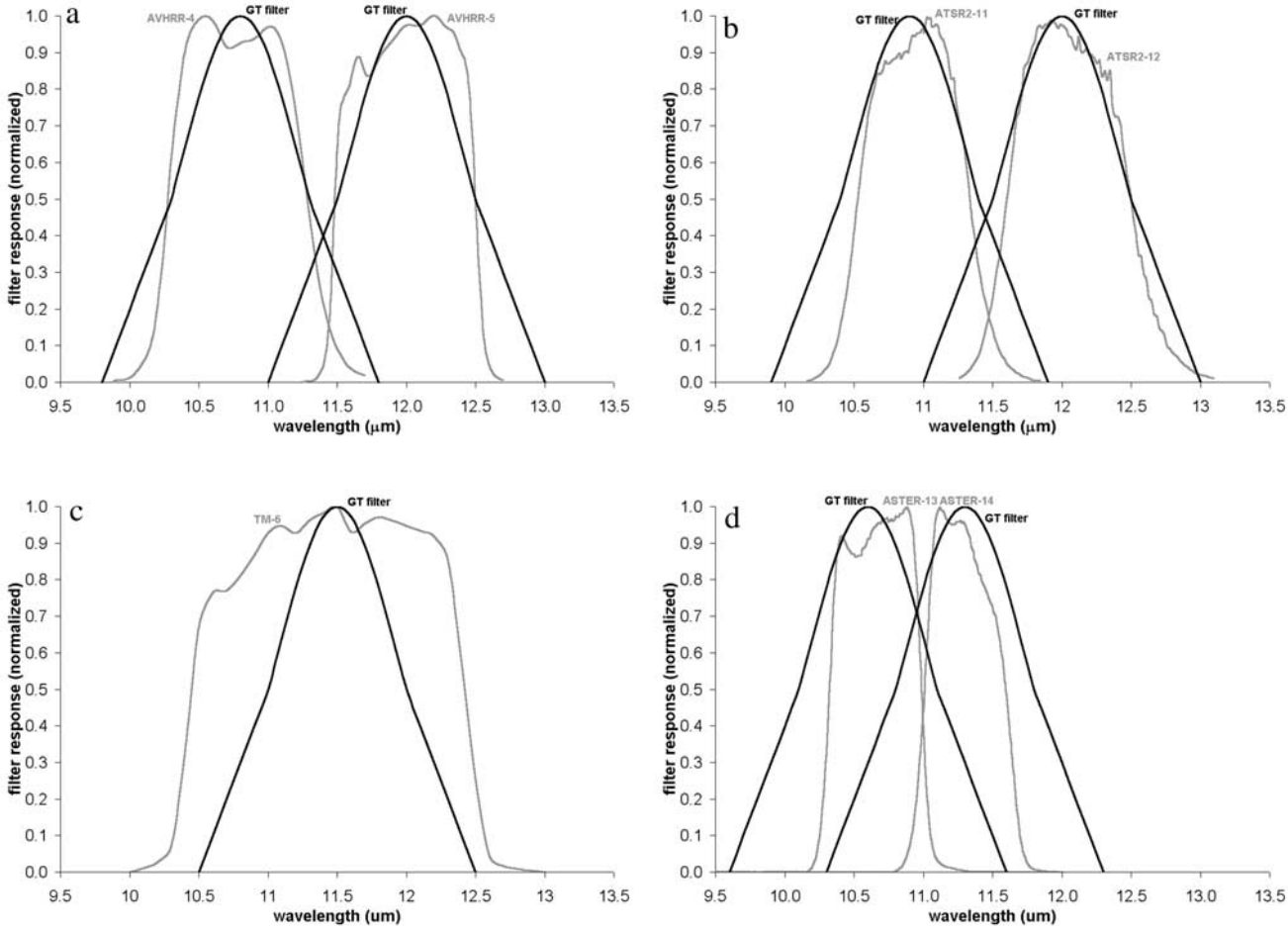

Figure 5. Comparison between the GT filter and (a) AVHRR 4 and 5 filters, (b) ATSR2 11 and 12 filters, (c) TM-6 filter and (d) ASTER 13 and 14 filters.

The same methodology proposed in section 3 can be used to obtain the explicit dependence on the wavelength and the atmospheric water vapour content for these atmospheric functions. The atmospheric function ψ_1^{SST} has the same expression and, therefore, the same numerical coefficients that the generalized algorithm. The atmospheric function ψ_2^{SST} can be obtained from Equation (12) and the following expressions with a correlation of 0.991 (in the region [10–12 μm]):

$$\eta_{2\lambda}^{SST} = -0.027015\,\lambda^3 + 0.82661\,\lambda^2 - 8.5005\,\lambda + 29.3086 \quad (18a)$$

$$\xi_{2\lambda}^{SST} = 0.12772\,\lambda^3 - 4.0027\,\lambda^2 + 42.0045\,\lambda - 147.7348 \quad (18b)$$

$$\chi_{2\lambda}^{SST} = -0.23034\,\lambda^3 + 7.1745\,\lambda^2 - 74.8482\,\lambda + 261.0593 \quad (18c)$$

$$\varphi_{2\lambda}^{SST} = 0.33896\,\lambda^3 - 11.4902\,\lambda^2 + 129.9832\,\lambda - 490.5483 \quad (18d)$$

7. Estimating the Wavelength for LST Retrieval

[29] The best wavelength to retrieve LST is the one for which the atmospheric transmissivity is maximum. To estimate this wavelength, the atmospheric function ψ_1 can be used, so this expression is the inverse of the atmopheric ttransmissivity (see Equation 7). In order to obtain this wavelength, the following condition must be applied:

$$\text{maximum/minimum} : \frac{d\psi_1}{d\lambda} = 0 \quad (19)$$

Taking into account the previous expression, it is possible to obtain the following equation, which must be solved to calculate the optimal wavelength (λ_{op}):

$$A(w)\lambda^2 + B(w)\lambda + C(w) = 0 \Rightarrow \lambda_{op}(w) = \frac{-B \pm \sqrt{B^2 - 4AC}}{2A} \quad (20)$$

where

$$A(w) \equiv 0.0027\,w^3 + 0.00096\,w^2 + 0.02958\,w - 0.46293 \quad (21a)$$

$$B(w) \equiv -0.03276\,w^3 - 0.12296\,w^2 - 0.47344\,w + 10.5514 \quad (21b)$$

$$C(w) \equiv 0.04745\,w^3 + 1.2021\,w^2 + 1.7133\,w - 60.1170 \quad (21c)$$

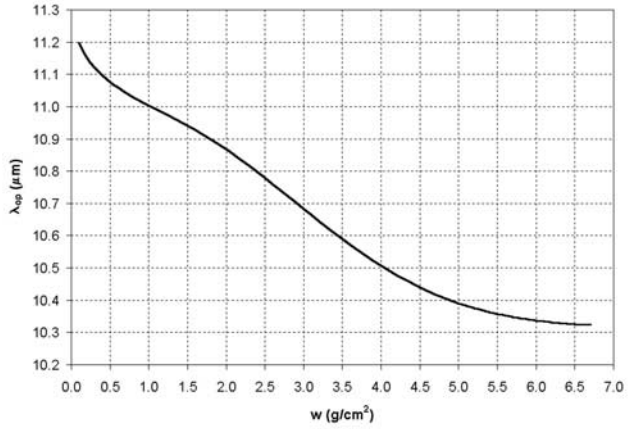

Figure 6. Effective optimal wavelength (λ_{op}) versus total atmospheric water vapor content.

It should be noted that maximum transmissivity values are obtained for minimum ψ_1 values, so to select one of the two possible solutions of the Equation (20) the following condition must be applied:

$$\text{minimum} : \frac{d^2\psi_1}{d\lambda^2} > 0 \qquad (22)$$

Figure 6 illustrates the graph of the effective λ_{op} versus the atmospheric water vapour content. The optimal wavelength values changes from 11.2 to 10.3 μm when the atmospheric water vapour changes between 0.1 and 6.7 g/cm^2. As an example, for atmospheric water vapour content of 1.0 g/cm^2, the best wavelength is 11.0 μm, while for a water vapour value of 4.0 g/cm^2, 10.5 μm is the best one.

8. Conclusions

[30] A generalized single-channel method has been developed to retrieve land surface temperature from remote sensing data for any thermal sensor with a full-width half-maximum value near to 1 μm and validated over different test sites. The best results are obtained for those thermal channels with effective wavelength near to 11 μm: for AVHRR-4, ATSR2-11 and TM-6 root mean square deviation values of 1.6 K, 2 K and 1.3 K have been obtained. Thermal channels with effective wavelength near to 12 μm provide worse results, with root mean square deviation values higher than 2 K for AVHRR-5 and ASTR2-12. Although theoretically the LST should be the same for different wavelengths, the higher absorption at wavelengths near to 12 μm in comparison with wavelengths near to 11 μm introduces higher errors on the LST retrieval, so the atmospheric correction is stronger. Higher errors are also introduced when the atmospheric water vapour content is greater: a rmsd lower than 1.8 K has been obtained from AVHRR-4 data acquired in the BOREAS experiment when the atmospheric water vapour content is less than 3 g/cm^2. However, values of rmsd between 3 K and 5 K are obtained when data acquired with atmospheric water vapour content greater than 3 g/cm^2 is included.

[31] Specific expressions have been found for Landsat TM-6, improving the rmsd values from 1.3 K with the generalized method to 0.5 K with the specific one (assuming a well calibration of the sensor). Finally, an estimation of the best wavelength to retrieve land surface temperature have been made, showing that this wavelength decreases with the atmospheric water vapour content. As an example, at 11 μm the transmissivity is maximum when the atmospheric water vapour content is 1 g/cm^2.

[32] **Acknowledgments.** We wish to thank to the European Union (WATERMED, project ICA3-ct-1999-00015) and the Ministerio de Ciencia y Tecnología (project REN2001-3105/CLI) for the financial support, and also to Guillem Sòria for his help.

References

Abreu, L. W., and G. P. Anderson (Eds.), The MODTRAN 2/3 report and LOWTRAN 7 model, *Modtran Rep.*, *Contract F19628-91-C-0132*, Phillips Lab., Hanscom Air Force Base, Massachusetts, 1996.

Barton, I. J., Satellite-derived sea surface temperatures: A comparison between operational, theoretical and experimental algorithms, *J. Appl. Meteorol.*, *31*, 432–442, 1992.

Becker, F., and Z.-L. Li, Towards a local split window method over land surfaces, *Int. J. Remote Sens.*, *11*, 369–394, 1990.

Becker, F., and Z.-L. Li, Surface Temperature and emissivity at various scales: Definition, measurement and related problems, *Remote Sens. Rev.*, *12*, 225–253, 1995.

Boluda, R., V. Andreu, M. Moraleda, and J. Sánchez, Factores ecológicos (geología, vegetación y clima) de la Comarca de La Plana de Requena-Utiel (Valencia), Vegetación y clima, in *Anal. Edafol. Agribiol.*, *47*, 903–917, 1998.

Dash, P., F.-M. Göttsche, F.-S. Olesen, and H. Fischer, Land surface temperature and emissivity estimation from passive sensor data: Theory and practice-current trends, *Int. J. Remote Sens.*, *23*, 2563–2594, 2002.

Gao, B. C., and F. H. Goetz, Column atmospheric water vapor and vegetation liquid water retrievals from airborne imaging spectrometer data, *J. Geophys. Res.*, *95*, 3549–3564, 1990a.

Gao, B. C., and F. H. Goetz, Determination of total column water vapor in the atmosphere at high spatial resolution from AVIRIS data using spectral curve fitting and band ratioing techniques, *SPIE Imaging Spectrosc. Terr. Environ.*, *1298*, 138–149, 1990b.

Gao, B. C., K. B. Heidebrecht, and F. H. Goetz, Derivation of scaled surface reflectance from AVIRIS data, *Remote Sens. Environ.*, *44*, 165–178, 1993.

Gillespie, A., S. Rokugawa, T. Matsunaga, J. S. Cothern, S. Hook, and A. B. Kahle, A temperature and emissivity separation algorithm for advanced spaceborne thermal emission and reflection radiometer (ASTER) images, *IEEE Trans. Geosci. Remote Sens.*, *36*, 1113–1126, 1998.

Goïta, K., and A. Royer, Surface temperature and emissivity separability over land surface from combined TIR and SWIR AVHRR data, *IEEE Trans. Geosci. Remote*, *35*, 1997.

Gu, D., and A. Gillespie, A new approach for temperature and emissivity separation, *Int. J. Remote Sens.*, *21*, 2127–2132, 2000.

Kaufman, Y. J., and B. C. Gao, Remote sensing of water vapor in the near IR from EOS/MODIS, *IEEE Trans. Geosci. Remote Sens.*, *30*, 1–27, 1992.

Lagouarde, J. P., Y. H. Kerr, and Y. Brunet, An experimental study of angular effects on surface temperature for various plant canopies and bare soils, *Agric. Forest Meteorol.*, *77*, 167–190, 1995.

May, D. A., L. L. Stowe, D. J. Hawkins, and E. P. McClain, A correction for Sahara dust effects on satellite sea surface temperature measurements, *J. Geophys. Res.*, *97*, 3611–3619, 1992.

Prata, A. J., Land surface temperatures derived from the advanced very high resolution radiometer and the along-track scanning radiometer, *J. Geophys. Res.*, *99*, 13,025–13,058, 1994.

Prata, A. J., Precipitable water retrieval from multi-filter rotating shadow-band radiometer measurements, *CSIRO Atmos. Res. Tech. Pap.*, no. 74, CSIRO, Australia, 2000.

Prata, A. J., and C. M. Platt, Land surface temperature measurements from the AVHRR, paper presented at the 5th AVHRR data users conference, Eur. Org. for the Exploit. of Meteorol. Satell., Tromso, Norway, 1991.

Price, J. C., Land surface temperature measurements from the split window channels of the NOAA 7 AVHRR, *J. Geophys. Res.*, *89*, 7231–7237, 1984.

Qin, Z., and A. Karnieli, Progress in the remote sensing of land surface temperature and ground emissivity using NOAA-AVHRR data, *Int. J. Remote Sens.*, *20*, 2367–2393, 1999.

Qin, Z., A. Karnieli, and P. Berliner, A mono-window algorithm for retrieving land surface temperature from Landsat TM data and its

application to the Israel-Egypt border region, *Int. J. Remote Sens.*, *22*, 3719–3746, 2001.

Schmugge, T., A. French, J. C. Ritchie, A. Rango, and H. Pelgrum, Temperature and emissivity separation from multispectral thermal infrared observations, *Remote Sens. Environ.*, *79*, 189–198, 2002.

Scott, N. A., and A. Chedin, A fast line by line method for atmospheric absorption computations: The authomatized atmospheric absorption atlas, *J. Meteorol.*, *20*, 802–812, 1981.

Sellers, O. J., et al., The Boreal Ecosystem Atmosphere Study (BOREAS): An overview and early results from the 1994 field year, *Bull. Am. Meteorol. Soc.*, *76*(9), 1549–1577, 1995.

Sobrino, J. A., and N. Raissouni, Toward remote sensing methods for land cover dynamic monitoring, Application to Morocco, *Int. J. Remote Sens.*, *20*, 353–366, 2000.

Sobrino, J. A., Z.-L. Li, and M. P. Stoll, Impact of the atmospheric transmittance and total water vapor content in the algorithms for estimating satellite sea surface temperatures, *IEEE Trans. Geosci. Remote Sens.*, *31*, 946–952, 1993a.

Sobrino, J. A., V. Caselles, and C. Coll, Theoretical split window algorithms for determining the actual surface temperature, *Il Nuovo Cim.*, *16*, 219–236, 1993b.

Sobrino, J. A., N. Raissouni, and A. Lobo, Monitoring the Iberian Peninsula land cover using NOAA-AVHRR data, in *Physical Measurements and Signatures in Remote Sensing*, edited by G. Guyot and T. Phulpin, pp. 787–794, A. A. Balkema, Brookfield, Vt., 1997a.

Sobrino, J. A., M. A. Olmeda, and N. Raissouni, Aplicación de la técnica de composición del máximo NDVI al seguimiento de la cobertura terrestre en la Península Ibérica, *Revista Teledetección*, *10*, 19–29, 1998.

Sobrino, J. A., J. El-Kharraz, and Z.-L. Li, Surface temperature and water vapour retrieval from MODIS data, *International J. Remote*, in press, 2003.

Sobrino, P., A. J. García Collado, J. A. Sobrino, and R. Boluda, Corrección atmosférica de imágenes Landsat-5 TM. Aplicación al estudio edafológico en la comarca de la Plana de Requena-Utiel, paper presented at VII Congreso Nacional de Teledetección, Santiago de Compostela, Asociac. Española de Teledetec., Cáceres, Spain, 1997b.

Ulivieri, C., M. M. Castronuovo, R. Francioni, and A. Cardillo, A split window algorithm for estimating land surface temperature from satellite, paper presented at COSPAR, Washington, D. C., 1992.

Ulivieri, C., M. M. Castronuovo, R. Francioni, and A. Cardillo, A split window algorithm for estimating land surface temperature from satellites, *Adv. Space Res.*, *14*(3), 59–65, 1994.

J. C. Jiménez-Muñoz and J. A. Sobrino, Global Change Unit, Department of Thermodynamics, Faculty of Physics, University of Valencia, S-46100, Burjassot, Spain. (jcjm@uv.es; jose.sobrino@uv.es)